Heliyon 5 (2019) e01489

Contents lists available at ScienceDirect

Heliyon

journal homepage: www.heliyon.com

Cerium doped $MgFe_2O_4$ nanocomposites: highly sensitive and fast response-recoverable acetone gas sensor

J.Y. Patil [a], D.Y. Nadargi [a], I.S. Mulla [b], S.S. Suryavanshi [a,*]

[a] School of Physical Sciences, Solapur University, Solapur 413255, India
[b] Former CSIR Emeritus Scientist, India

ARTICLE INFO

Keyword:
Materials science

ABSTRACT

We report a facile synthesis of Cerium doped $MgFe_2O_4$ nanocomposite ferrite and its usability as gas-sensor via simple and robust synthesis approach of glycine-combustion-process. The route utilizes metal nitrates (Ce, Mg, Fe -nitrates) and glycine, in aqueous solution. The involved sol-gel concept was explained on the basis of zwitterion characteristic of glycine. The analysis of the developed ferrite was done in two different ways – i) effect of Ce-doping concentration, and ii) effect of sintering temperature. With the ferrite system $MgFe_{2-x}Ce_xO_4$, the doping concentration of Ce was varied from 0.04 to 0.12 with the step x = 0.04, and sintering was done at two different temperatures i.e. 973K and 1173K. As-produced composite system was examined for their gas response towards reducing gases such as LPG, ethanol, acetone and ammonia. The material displayed excellent gas sensing properties towards acetone for wide operating temperature range of 575–675 K. The XRD analysis revealed nanocrystallinity with crystallite size in the range of 28–34 nm. Microstructural analysis confirmed the porous morphology due to auto-ignition during the combustion reaction. The present investigations confirm the produced $MgFe_{2-x}Ce_xO_4$ is a promising candidate for fabricating high performance acetone sensor.

1. Introduction

Gas sensors have become an integral part of the modern civilization due to their key role in detecting, monitoring, and controlling the hazardous/poisonous gases from the surrounding. Acetone is a very common volatile organic compound (VOC), which is extensively used as reagent in laboratories and industry. Since, acetone easily evaporates are at room temperature (BP = 56.53 °C), its safety concerns are of high importance to take care. It may cause many health hazard issues to human, such as headache, narcosis, etc. at concentration higher than 500 ppm. Moreover, the mixture of its vapor and the air will explode when the volume concentration of acetone is in the range of 2.6–12.8% [1]. Moreover, the concentration of acetone exhaled by Type-I diabetic patients is higher than that of healthy people. It is a selective breath marker for Type-1 diabetes. A healthy/normal person breath has less than 0.9 ppm concentration of acetone. If this level double-up (1.8 ppm), giving the signs of ketosis (high ketone level in blood) of insulin-dependent diabetes. Thus, highly sensitive and selective sensors for acetone detection are required for the rapid assessment of diabetes and related diseases [2].

Ferrite compounds are very important materials due to their semiconducting and ferrimagnetic properties. Recently spinel ferrites have been found as perspective gas sensor materials at elevated temperatures [3, 4, 5, 6, 7, 8]. However, the researchers are still facing cross sensitivity toward non-targeted gases, high sensitivity to humidity, long term drift towards oxygen bulk diffusion, and transformations of the crystal structure in polycrystalline materials, are the major ones [9, 10, 11]. In order to overcome the aforementioned hurdles, inert impurities will be the most suitable solution. To enhance the catalytic performance, noble metals and transition metal oxides can be utilized. They not only modify catalytic activity of ferrite material, but also enhance the concentration of charge carriers and physicochemical properties [12, 13, 14, 15, 16, 17]. Alkali and alkaline earth metals are known as electron exchange promoters, presumably because of the higher partial charge on the neighboring oxygen. In contrast, transition and rare earth metals are the promoters of active sites formation [18]. Focusing on rare earth cations (usually trivalent cations), they influence the materials' electronic distribution, favoring the adsorption of oxygen species [19, 20]. These metals are little explored as dopants for the improvement in the catalytic properties of the ferrite material. This is one of the motivations, behind using Ce rare earth cation in the present ferrite system. Both intrinsic and extrinsic oxygen vacancies exist in ceria, thus provide the passage for oxide ion hopping. The intrinsic vacancies arise from the presence of

* Corresponding author.
E-mail address: sssuryavanshi@rediffmail.com (S.S. Suryavanshi).

https://doi.org/10.1016/j.heliyon.2019.e01489
Received 27 November 2018; Received in revised form 19 February 2019; Accepted 4 April 2019

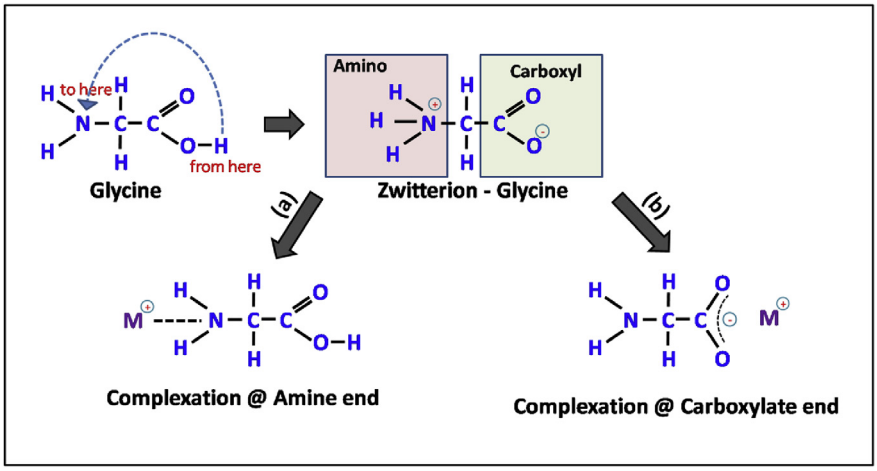

Fig. 1. Initial stages of glycine-metal complexation in an aqueous solution. Complexation can involve either, amine end (part a) or carboxylate end (part b) of the glycine molecule.

Ce^{3+} ions in the fluorite lattice due to the reduction equilibrium of Ce^{3+}/Ce^{4+}, whereas extrinsic vacancies arise by the substitution of aliovalent ions in the lattice [21]. These properties favor the oxygen adsorptive capacity of pristine ferrite material, to improve the gas sensing performance.

In the present work, we demonstrate the facile and flexible strategy of fabricating cerium doped magnesium ferrite via traditional glycine-gel combustion process, and its use as gas sensor for various reducing gases. The selected combustion route and the choice of fuel for combustion process is more favored, as it has high negative combustion heat (−3.24 kcal/g) compared to other possible combustive fuels (urea: −2.98 kcal/g, citric acid: −2.76 kcal/g) [22]. Further, as transition metals are most effectively complexed by the amine group, use of glycine as a fuel has an added value. It is helpful not only in preventing the selective precipitation but also allows effective complexation with metal cations, during the complexation process of ferrite metal ions with cerium due to zwitterionic character [23]. Sufficient degree of crystallization and structural evolution is required to attain desired electronic properties which are necessary for gas sensor application. Therefore, effect of sintering temperature on physico-chemical properties of as-developed

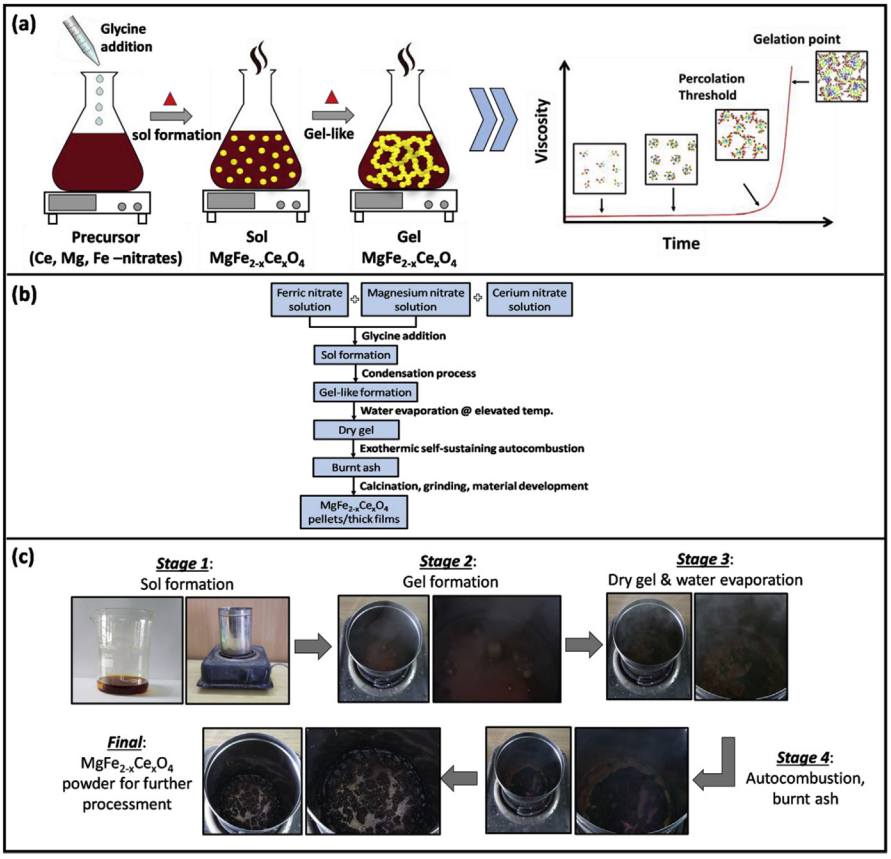

Fig. 2. Schematic of complete experimental procedure. a) illustration of sol-gel combustion reaction along with the viscosity graph, b) experimental flowchart, c) photographs of transitional steps from reactants to final product.

material is also discussed. The structural and morphological investigations are discussed on the context of ferrite preparation strategy and amount of cerium doping.

2. Experimental

The general approach of developing cerium doped $MgFe_2O_4$ involves following two major steps: (i) synthesis of material powder by sol–gel autocombustion process and formation of pellets and/or thick films, (ii) investigation/characterization of the developed ferrite material.

2.1. Synthesis of ferrite material ($MgFe_{2-x}Ce_xO_4$ with $x = 0.04, 0.08, 0.12$)

In a typical synthesis, AR grade nitrates (magnesium nitrate ($Mg(NO_3)_2.6H_20$), ferric nitrate ($Fe(NO_3)_2.9H_20$), cerium nitrate ($Ce(NO_3)_3.6H_20$)), and glycine (NH_2CH_2COOH) obtained from Sigma Aldrich, were used as received. The ratio of valencies of metal nitrate to glycine which provides the maximum exothermic reaction during the combustion process was kept constant at 3:5. In the present ferrite system of $MgFe_{2-x}Ce_xO_4$, the doping concentration of Ce was varied from 0.04 to 0.12 with the step x = 0.04. The synthetic reagents were well mixed in the suitable amount of distilled water (~100ml). The reaction mixture was stirred for ample time, till it attained the homogeneous phase. The temperature of solution was eventually raised up to 425 K. In the process, the glycine (amino acid) plays two importance roles. Primarily, it acts as bidentate ligand (i.e. a ligand with two "teeth" or atoms that coordinate directly to the central metal atom). In the present case, a single molecule of glycine can form two bonds to a metal ion, forming a complex with the metal ions. Secondly, it boosts the solubility of the metal ions. Therefore, it can restrict the selective precipitation (if any) upon evaporation of water during combustion process. For the complex formation, glycine has dual end groups (carboxylic and amino), where both end groups can be utilized. Due to this zwitter (Zwitter in German, stands for "Dual") characteristic, glycine is referred as zwitter-ions, which facilitates effective complexation with metal ions of varying ionic sizes. The said characteristic of glycine in the aforementioned in forming a stable metal complex is depicted in the following Fig. 1.

In accordance with the natural behavior, the viscosity of the solution increased gradually by the evaporation of water molecules, and ended-up in a gel. The resultant gel was continued to heat treat at slightly higher temperature (450–575 K). The viscous gel began frothing and eventually after water evaporation, the gel started exhausting into fast flameless auto combustion reaction with the evolution of large amount of gaseous products, after which it gets auto ignited. The said process is self-sustaining and highly exothermic in nature. This ensured the formation and crystallization of the designed metal oxide powders. As-obtained raw powder was calcined at 775 K in air for 2h, to eliminate the traces of unreacted left-overs. The calcined powder was then made into pellets and thick films. The process of developing pellets and thick films is described below [24, 25]. In the end, both pellets and thick films were sintered at 975 K and 1173 K for 2 h in air. Fig. 2 illustrates the complete experimental scheme along with the photographs of transitional steps.

2.1.1. Thick films process details

The thixotropic paste of ferrite material was formulated by mixing calcined fine powder of pristine and Ce doped ferrite with a mixture of temporary binder (ethyl cellulose and butyl carbitol acetate). In formulating the paste; inorganic to organic part was taken in the weight ratio of 75:25. This paste was deposited on to the ultrasonically cleaned alumina substrate (5 mm × 10 mm) using screen printing technique with nylon cloth of 140 mesh counts. The typical thickness of the films was ~10 μm.

2.1.2. Pellets fabrication details

The calcinated ferrite powder was made into pellets (15mm diameter and 2mm thickness) with manual pressing machine at the pressure of 1.5 t/cm^2 using polyvinyl alcohol as a binder.

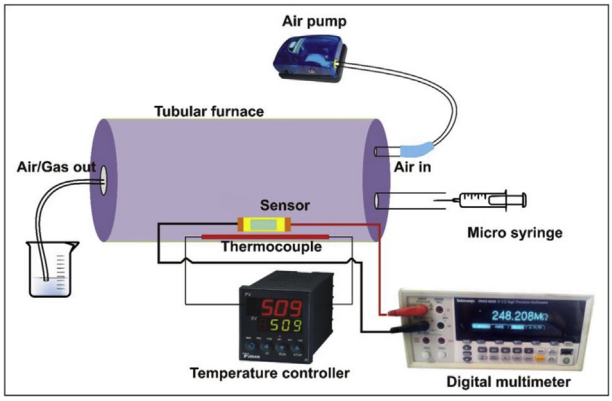

Fig. 3. An indigenous dynamic gas sensing set-up utilised for gas sensing analysis. The gas response was calculated by the formula highlighted in Eq. (1).

2.2. Investigation/characterization of the material

The structural study of the $MgFe_{2-x}$ Ce_xO_4 (x = 0.04, 0.08, 0.12) material was done using the X-ray diffractometer (PHILIPS PW-3710) with Cu-K_α line at 0.15056 nm. The surface morphological images of the sintered pellets and thick films were taken using field emission scanning electron microscope (FESEM, Tescan, JMIRA3 LM model, USA).

The reducing gas sensing properties of as-prepared magnesium ferrite was studied in the dynamic mode. An indigenous dynamic gas sensing set-up (Fig. 3) was utilised for analysing the developed ferrite for gas sensing application. It consists of a test gas chamber (2 Lit.) in which a sensor material (thick film/pellet) is rested on the sample holder. The temperature of the sensor can be regulated through a temperature controller using a heating coil and a thermocouple. Change in resistance of sensor for the specific test gas was measured by digital multimeter (Tektronix DMM 4050 6-1/2 digit precision multimeter) at its prerequisite concentration. The temperature of the system was controlled from room temperature to 725K within the precision of ±274.15K, and the electrical resistance was calculated. Conducting silver paste was applied to make electrical contacts on both ends of thick film. Two probe ceramic sample holder was used to mount the sensor material in an insulated glass tube chamber which was installed coaxially in a tubular furnace. The sensor material area was kept constant for all samples prepared for the measurements. In order to inject the test gas, Teflon plunger plastic syringe of 2 ml and 1 ml (with least count of 0.1 ml)

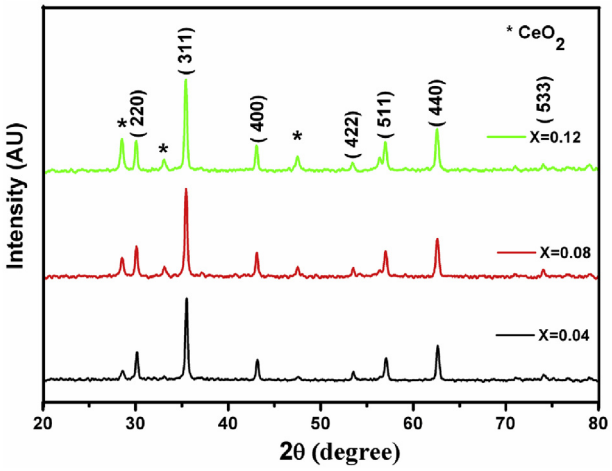

Fig. 4. The XRD pattern of sintered $MgFe_{2-x}$ Ce_xO_4 (x = 0.04, 0.08, 0.12) samples.

Table 1
Crystallite size and lattice parameter of $MgFe_{2-x}Ce_xO_4$ (x = 0.04, 0.08, 0.12).

#	Sample Name	Crystallite size (nm)		Lattice parameter of sintered sample (Å)
		As-synthesized	sintered	
1	$MgFe_{1.96}$ $Ce_{0.04}$ O_4	31	34	8.361
2	$MgFe_{1.92}$ $Ce_{0.08}$ O_4	29	32	8.389
3	$MgFe_{1.88}$ $Ce_{0.12}$ O_4	28	31	8.391

capacity was utilized. The known amount of test gas was interjected in the gas-mixing chamber so that their required part per million (ppm) levels is attained. The resistance of the sensor was calculated as a function of time at different operating temperatures and concentrations of test gas.

$$S(\%) = \frac{(R_a - R_g)}{R_a} \times 100 \quad (1)$$

Where, R_a is resistance of sensor in air and R_g resistance in presence of test gas.

3. Results and discussion

3.1. Crystallographic identification

The crystal structure of calcined samples was confirmed by grazing incidence X-ray diffraction (XRD). Fig. 4 shows the XRD pattern of $MgFe_{2-x}Ce_xO_4$ (x = 0.04, 0.08 and 0.12). As expected, the ferrite composite showed the exact same Bragg reflection signatures which are typical for the spinal $MgFe_2O_4$ structure. The relative intensities of the various reflections arising from the various crystal plane reflections (220), (311), (400), (422), (511) and (440) also correspond to those of the spinel reference (JCPDS files No. 73–1720 for $MgFe_2O_4$). In addition, weak peaks corresponding to CeO_2 were also reflected in the XRD signatures. As Ce-doping increased, the crystallite size got decreased gradually. This was revealed in the XRD pattern, where CeO_2 peaks get shifted towards the right side, as θ value was increased. At lower dopant levels, Ce was incorporated primarily by the substitution of Fe atoms in the crystal lattice. Therefore, the peaks of CeO_2 at 0.04 mol%, are just visible. In contrast, CeO_2 at higher doping level (0.12 mol%), the peak intensity is prominent.

The *d*-spacing and average lattice parameter values are consistent with those given in the JCPDS files $MgFe_2O_4$ (No. 73–1720). The average crystallite size (calculated using peak broadening of most intense peak) and the average lattice parameter of annealed sample (calculated using the interplanar spacing formula) are tabulated in the following Table 1. From the table, it is seen that the crystallite size increased after sintering. It is known that ferrites generally need high temperature for the formation of single phase spinel structure. However by employing the present method, it can be synthesized at relatively lower temperature with lesser processing time.

3.2. Surface morphological properties and EDS studies

Fig. 5 shows the surface topography (FE-SEM images) of Ce incorporated $MgFe_2O_4$ ferrite (pellets and thick films). In general, the ferrite structure was significantly influenced by addition of Ce and sintering

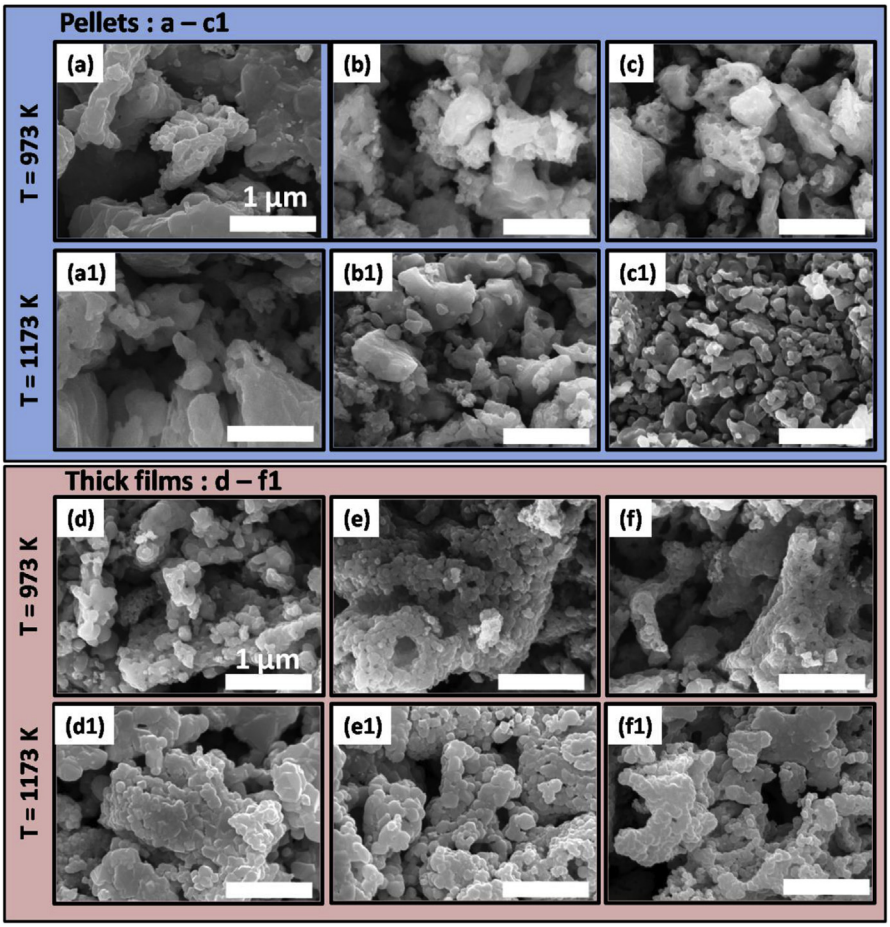

Fig. 5. FE- SEM micrographs of $MgFe_{2-x}Ce_xO_4$ (x = 0.04, 0.08, 0.12) at different sintering temperatures and material fabrication. a-c1: pellet samples, d-f1: Thick film samples.

Table 2
Energy Dispersive X-ray analysis of $MgFe_{2-x}Ce_xO_4$ (x = 0.04, 0.08, 0.12) samples sintered at 973 K.

Element	$MgFe_{1.96}Ce_{0.04}O_4$				$MgFe_{1.92}Ce_{0.08}O_4$				$MgFe_{1.88}Ce_{0.12}O_4$			
	Pellets		Thick films		Pellets		Thick films		Pellets		Thick films	
	Wt (%)	At (%)	Wt (%)	At (%)	Wt (%)	At (%)	Wt (%)	At (%)	Wt (%)	At (%)	Wt (%)	At (%)
O	20.35	42.45	17.50	38.72	21.58	45.05	18.31	40.43	18.98	41.99	19.11	42.28
Mg	13.95	19.17	12.59	18.35	13.45	18.47	12.66	18.38	12.41	18.08	12.38	18.02
Ce	2.48	0.59	3.59	0.91	6.62	1.59	6.46	1.64	9.37	2.38	9.81	2.47
Fe	63.22	37.79	66.32	42.02	58.35	34.89	62.55	39.55	59.24	37.55	58.70	37.23

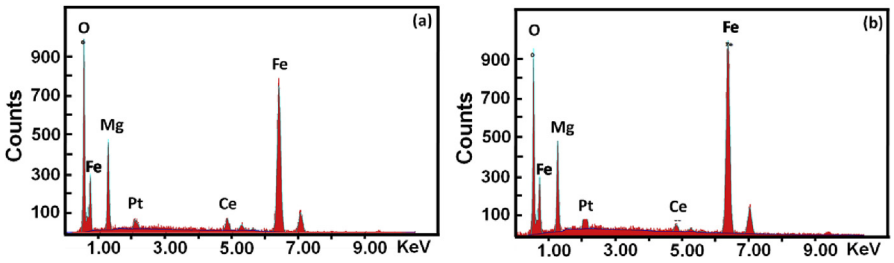

Fig. 6. EDS spectrum of $MgFe_{1.96}Ce_{0.04}O_4$ sintered at 973 K, a: pellet and b: thick films.

temperature. A network of particles was observed in all the prepared samples, which is typical in case of sol-gel derived materials. The morphology of the pellets is depicted in Fig. 5 a-c1, whereas thick films are highlighted in Fig. 5 d-f1. The pellets sintered at 973 K (Fig. 5 a-c) illustrated the formation of highly porous structure with surface voids. Moreover, partially developed grains with no particular morphology were seen. The observed porous microstructure is useful for gas sensing applications, as gas sensing is a surface phenomenon and porosity plays a crucial role. With an increase in the sintering temperature (1173 K, Fig. 5 a1-c1), the morphology of the pellets get modified considerably. Fully

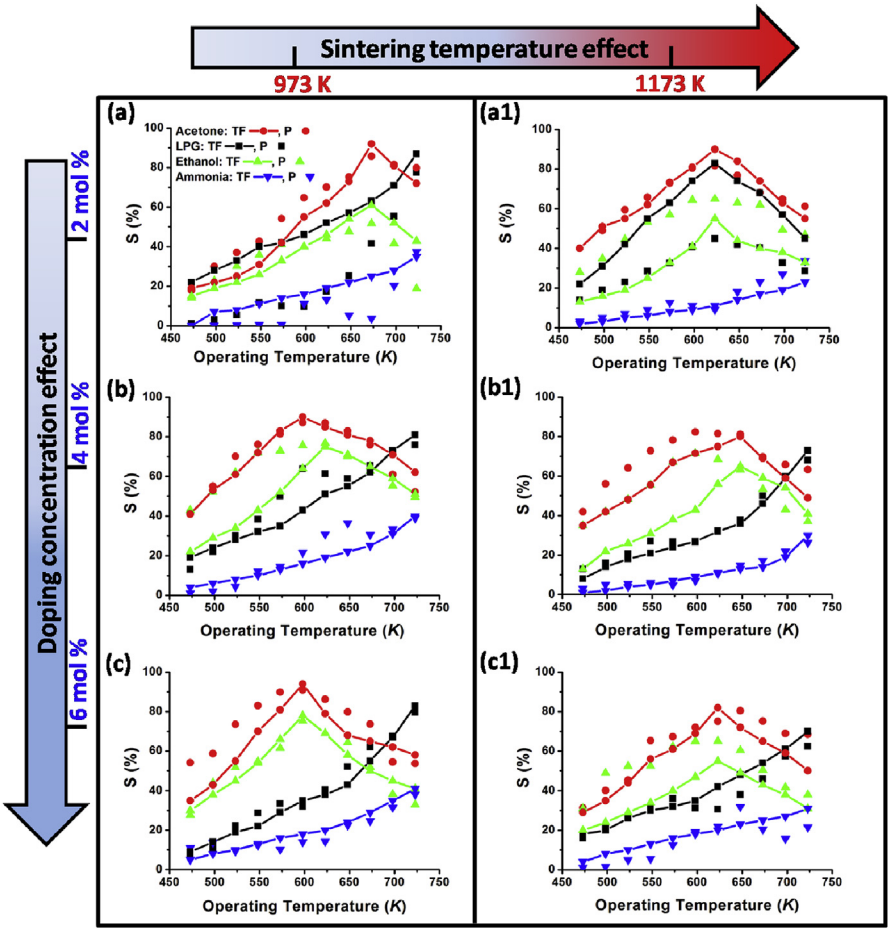

Fig. 7. Response of $MgFe_{2-x}Ce_xO_4$ (x = 0.04, 0.08, 0.12) samples at different operating temperature. a&a1: $MgFe_{1.96}Ce_{0.04}O_4$, b&b1: $MgFe_{1.92}Ce_{0.08}O_4$, c&c1: $MgFe_{1.88}Ce_{0.12}O_4$.

Table 3
Effect of Ce-doping and sintering temperature on optimum operating temperature and gas response of as-developed material.

#	Test gas	Sintering effect (K) ↓	Ce - doping effect →					
			x = 0.04		x = 0.08		x = 0.12	
			Opt. temp. (K)	Gas res. (%)	Opt. temp. (K)	Gas res. (%)	Opt. temp. (K)	Gas res. (%)
1	Acetone		**Pellet**					
		973	673	86	598	87	598	91
		1173	623	82	623	82	648	81
			Thick film					
		973	673	92	598	90	598	94
		1173	623	90	648	80	623	82
2	LPG		**Pellet**					
		973	723	78	723	76	723	80
		1173	623	82	723	68	723	62
			Thick film					
		973	723	87	723	81	723	83
		1173	623	83	723	73	723	70
3	Ethanol		**Pellet**					
		973	673	58	623	77	598	75
		1173	623	63	598	71	623	65
			Thick film					
		973	673	61	623	75	598	78
		1173	623	55	648	65	623	55
4	Ammonia							
		973	723	37	723	39	723	38
		1173	723	33	698	26	723	21
			Thick film					
		973	723	35	723	40	723	41
		1173	723	23	723	30	723	31

developed grains were observed, and the average grain size was found to be 0.24, 0.13 and 0.07 μm, as amount of Ce doping increased from x = 0.04–0.12.

Unlike pellets, the well developed grains were obtained in case of thick films sintered at 973K. The average grain size was found to decrease, with increase in the Ce-doping. The obtained values are 0.27, 0.24 and 0.09 μm with increasing Ce concentration from x = 0.04–0.12 mol%. The said behavior is attributed to secondary phase formation of CeO_2 which hinders the grain growth. The similar results were obtained to Rezlescu et al., wherein 2 wt% Ce doped material exhibited well developed grains, and their grain size decreases with the increasing concentration of CeO_2 [26]. As expected, with an increase in the sintering temperature (1173 K), the morphology of the films was modified. The network connectivity was well developed, favoring the larger porosity and hence the higher surface, which leads to better adsorption of oxygen and test gases. The positive consequences were seen in gas sensing response, where the sensitivity got boosted when the same sensing material was transformed from pellet (lower surface area) to thick films (higher surface).

Table 2 shows the EDS data of all the ferrite samples (pellets and thick films) sintered at 973 K. The values are in good agreement with the initial precursor concentration and show nearly 1:2 atomic ratio of Mg and Fe with slightly lower oxygen concentration, indicating the formation of composite ferrite of cerium. Further, with the increasing doping concentration, the atomic percentage of the Ce was found to increase. Fig. 6 shows the EDS spectra of $MgFe_{1.96}Ce_{0.04}O_4$ ferrite sample (a: Pellet, b: Thick film) sintered at 973 K. In both the cases, the EDS spectrum confirms the presence of constituent elements (Mg, Fe, O and Ce) without any impurity.

3.3. Sensor analysis

Following to the crystallographic and morphological analyses, the developed materials were tested for the gas sensing application. Primarily, optimum working temperature in both, pellet and thick film, at different sintering temperature and doping concentration was investigated. Later, the material was (pellets and thick films) analyzed for its sensitivity at different concentrations of the test gases, at their optimum operating temperature.

3.3.1. Optimum working temperature investigation

The response as a function of operating temperature for all the ferrite samples is shown in Fig. 7. The respective arrow-direction indicates the response behavior in two directions - doping concentration level and -sintering temperature. Dots-without-line represents pellet, whereas dots-with-line represents thin film samples. The gas response was tested at 2000 ppm concentration of different reduced gases viz. acetone, ammonia, ethanol and LPG. In general, the material showed highest response towards acetone amongst the investigated reduced gases. In correlation with the obtained morphology (seen in the SEM) and theoretical background, thick films were expected to have better gas sensing response than that of pellets. However, the response curves showed marginal difference between pellets and thick films sensing material. Nevertheless, to underline the sentence, the response and recovery time was significantly improved in thick films case, which is discussed later in the section of response and recovery time studies.

It is obvious that, the sensor with lower operating temperature is preferable, than higher operating temperature ones. In the present study, it was observed that the operating temperature reduced with increasing Ce-doping upto 0.08 mol% for acetone gas. It showed reduction from 673 K to 598 K optimum operating temperature for acetone. However, with further increase in the doping concentration (x = 0.12), the material remained at the lower shift of optimum operating temperature (i.e. 598 K). Therefore, the doping above x = 0.12 were not conducted for acetone gas testing. However, for ethanol gas sensing, the material showed reducing nature of optimum operating temperature with increasing doping concentration upto 0.12 mol%. It reduced from 673K to 598K, with increasing doping concentration from 0.04 mol% to 0.12 mol%. Nevertheless, on comparing with acetone sensing, the material showed lower response for ethanol. Therefore, further doping concentrations to reduce the operating temperature for ethanol sensing, were not conducted. In case of ammonia and LPG, a gradual increase in the gas response was observed with increasing operating temperature upto 725K, which is inappropriate for ideal gas sensor. Therefore, the response characteristics for ammonia and LPG gas after 725K were not entertained further.

Table 4
Response and Recovery time of as prepared Ce-doped $MgFe_2O_4$ sensing material.

#	Test gas	Sintering effect (K)	Ce - doping effect →					
			x = 0.04		x = 0.08		x = 0.12	
			Response time (Sec.)	Recovery time (Sec.)	Response time (Sec.)	Recovery time (Sec.)	Response time (Sec.)	Recovery time (Sec.)
1	Acetone		**Pellet**					
		973	21	29	29	51	43	92
		1173	16	24	23	26	29	57
			Thick film					
		973	13	20	21	15	20	65
		1173	10	14	14	11	17	27
2	LPG		**Pellet**					
		973	42	31	47	45	51	63
		1173	33	28	34	29	40	37
			Thick film					
		973	20	25	37	23	30	42
		1173	16	24	22	19	21	16
3	Ethanol		**Pellet**					
		973	9	20	15	31	38	84
		1173	7	16	13	19	31	50
			Thick film					
		973	7	17	11	9	18	57
		1173	5	12	8	7	15	31
4	Ammonia		**Pellet**					
		973	15	35	22	39	29	38
		1173	6	11	16	9	20	8
			Thick film					
		973	11	22	15	8	11	21
		1173	7	15	9	5	9	8

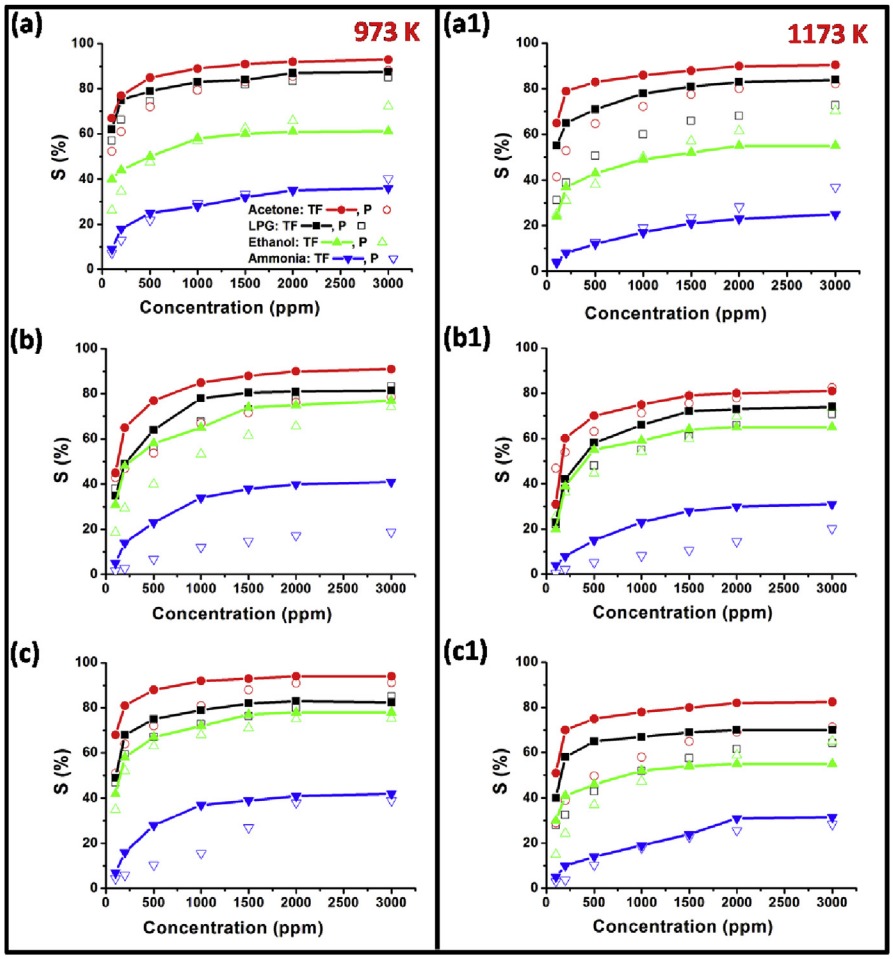

Fig. 8. Response of $MgFe_{2-x}Ce_xO_4$ (x = 0.04, 0.08, 0.12) samples at different gas concentration. a&a1: $MgFe_{1.96}Ce_{0.04}O_4$, b&b1: $MgFe_{1.92}Ce_{0.08}O_4$, c&c1: $MgFe_{1.88}Ce_{0.12}O_4$.

The sensors showed marginal difference between the two sintering temperatures i.e. at 973K and 1173K. The sensor with Ce doping of 0.04 mol% showed decrease in the optimum operating temperature (from 675 K to 625 K) upon sintering at elevated temperature, 1173K. However, the gas response was reduced by 4%. In conclusion, the sintering temperature at 973K is more suitable for the sensing characteristics of the material.

Table 3 shows tabulated results of gas response for various Ce doped samples at different operating temperatures.

3.3.2. Response and recovery time measurement

In the context of availing the advantage of increasing surface area (from pellets to thick films) for better gas sensing intention, the response and recovery time was investigated. Though there was no drastic enhancement in the sensitivity by increasing the surface area, the response and recovery time values shows remarkable improvement in the thick films as compared with pellets. Following Table 4 shows the values of improved response and recovery time of as prepared sensing material.

3.3.3. Gas response analysis at various concentration of test gases

At an optimized operating temperature, the sensors' response towards the aforementioned reducing gases with varying concentrations (100–3000 ppm) is depicted in Fig. 8. There is not much difference between the samples sintered at 973K (Fig. 8: left part) and 1173 (Fig. 8: right part). In general, the sensor response towards acetone is higher than other three reduced gases (ammonia, LPG, and ethanol). The gas response initially increases linearly with the concentration of test gas due to increased interactions of the gas molecules with the available active surface area, thereafter on reaching at the optimum concentration, it gets saturated and shows nearly similar response. The sensor response is given by the following formula highlighted in Eq. (2) [27]:

$$S = X[Y]^n + K;\ (n = 0.5\ to\ 1.0) \quad (2)$$

Where, X and K are constants, Y is the concentration of test gas. The value of integer n can have any value between 0.5-1.0; according to reaction stoichiometry and surface species charge. This linear relationship is a key prerequisite condition in case of several applications like on-line gas monitoring [25].

4. Conclusions

In conclusion, we demonstrated the facile and flexible strategy of fabricating cerium doped magnesium ferrite via traditional glycine-gel combustion process, and its use as gas sensor for various reducing gases (ethanol, acetone, ammonia, and LPG). The developed material was characterized in two different directions – i) effect of Ce-doping concentration, and ii) effect of sintering temperature. The gas response was related to the form of the material (pellet and thick film), doping concentration, sintering temperature, operating temperature, gas type and porosity of the ferrite. The well developed grains were obtained in thick films than in pellets. Hence, the gas response was obtained better in thick films, due to increased surface area. There was marginal improvement in the gas sensing at elevated sintering temperature (i.e. at 1173K). The material displayed excellent gas sensing properties towards acetone, and for wide operating temperature range (575–675 K). Though there was no drastic enhancement in the sensitivity by increasing the surface area, the response and recovery time values shows remarkable improvement in the thick films as compared with pellets. The sensors material showed good reproducibility even after 4 months with 8% decrement in the response. The reported approach of fabricating gas sensor is easily reproducible at relatively lower cost and thus offers great promise for future industrial application of gas sensors.

Declarations

Author contribution statement

J. Y. Patil: Performed the experiments; Wrote the paper.

D. Y. Nadargi, I. S. Mulla: Analyzed and interpreted the data; Contributed reagents, materials, analysis tools or data.

S. S. Suryavanshi: Conceived and designed the experiments.

Funding statement

This research did not receive any specific grant from funding agencies in the public, commercial, or not-for-profit sectors.

Competing interest statement

The authors declare no conflict of interest.

Additional information

No additional information is available for this paper.

References

[1] Li Jiao, Pinggui Tang, Jiajun Zhang, Yongjun Feng, Ruixian Luo, Aifan Chen, Dianqing Li, Facile synthesis and acetone sensing performance of hierarchical SnO_2 hollow microspheres with controllable size and shell thickness, Ind. Eng. Chem. Res. 55 (12) (2016) 3588.

[2] S. Singkammo, A. Wisitsoraat, C. Sriprachuabwong, A. Tuantranont, S. Phanichphant, C. Liewhiran, Electrolytically exfoliated graphene-loaded flame-made Ni-doped SnO_2 composite film for acetone sensing, ACS Appl. Mater. Interfaces 7 (5) (2015) 3077.

[3] Alaud Din, Kalsoom Akhtar, Kh. S. Karimov, Noshin Fatima, Abdullah M. Asiri, M.I. Khan, Sher Bahadar Khan, Fe_2O_3-Co_3O_4 nanocomposites based humidity and temperature sensors, J. Mol. Liq. 237 (2017) 266.

[4] Safi Asim Bin Asifa, Sher Bahadar Khan, Abdullah M. Asiri, Assessment of graphene oxide/MgAl oxide nanocomposite as a non-enzymatic sensor for electrochemical quantification of hydrogen peroxide, J. Taiwan Inst. Chem. Eng. 74 (2017) 255.

[5] Alaud Din, Kh. S. Karimov, Kalsoom Akhtar, M.I. Khan, Muhammad Tariq Saeed Chani, Murad Ali Khan, Abdullah M. Asiri, Sher Bahadar Khan, Impedimetric humidity sensor based on the use of SnO_2–Co_3O_4 spheres, J. Mater. Sci. Mater. Electron. 28 (2017) 4260.

[6] Alaud Din, Sher Bahadar Khan, M.I. Khan, Safi Asim Bin Asif, Murad Ali Khan, Saima Gul, Kalsoom Akhtar, Abdullah M. Asiri, Cadmium oxide based efficient electrocatalyst for hydrogen peroxide sensing and water oxidation, J. Mater. Sci. Mater. Electron. 28 (1) (2017) 1092.

[7] Muhammad Tariq Saeed Chani, Khasan S. Karimov, Sher Bahadar Khan, Abdullah M. Asiri, Fabrication and investigation of cellulose acetate-copper oxide nanocomposite based humidity sensors, Sensor Actuator Phys. 246 (2016) 58.

[8] Sher Bahadar Khan, Khasan S. Karimov, Muhammad Tariq Saeed Chani, Abdullah M. Asiri, Kalsoom Akhtar, Noshin Fatima, Impedimetric sensing of humidity and temperature using CeO_2–Co_3O_4 nanoparticles in polymer hosts, Microchimica Acta 182 (11-12) (2015) 2019.

[9] P.J.D. Peterson, A. Aujla, K.H. Grant, A.G. Brundle, M.R. Thompson, J.V. Hey, R.J. Leigh, Practical use of metal oxide semiconductor gas sensors for measuring nitrogen dioxide and ozone in urban environments, Sensors 17 (2017) 1653.

[10] G. Korotcenkov, Gas response control through structural and chemical modification of metal oxide films: state of the art and approaches, Sensor. Actuator. B 107 (2005) 209.

[11] C.C. Wang, A.A. Akbar, M.J. Madou, Ceramic based resistive sensors, J. Electroceram. 2 (4) (1998) 273.

[12] T. Skala, K. Veltruska, M. Moroseac, I. Matolinova, G. Korotcenkov, V. Matolin, Study of Pd–In interaction during Pd deposition on pyrolytically prepared In_2O_3, Appl. Surf. Sci. 205 (2003) 196.

[13] F. Kawamura, I. Yasui, M. Kamei, I. Sunagawa, Habit modifications of SnO_2 crystals in SnO_2–Cu_2O flux system in the presence of trivalent impurity cations, J. Am. Ceram. Soc. 84 (2001) 1134.

[14] D. Szezuka, J. Werner, S. Oswald, G. Behr, K. Wetzig, XPS investigations of surface segregation of doping elements in SnO_2, Appl. Surf. Sci. 179 (2001) 301.

[15] G. Korotcenkov, A. Cerneavschi, V. Brinzari, A. Vasiliev, A. Cornet, J. Morante, A. Cabot, J. Arbiol, XPS investigations of surface segregation of doping elements in SnO_2, Sensor. Actuator. B 99 (2/3) (2004) 304.

[16] E.R. Leite, I.T. Weber, E. Longo, J.A. Varela, A new method to control particle size and particle size distribution of SnO_2 nanoparticles for gas sensor applications, Adv. Mater. 12 (13) (2000) 965.

[17] F. Lu, Y. Liu, M. Dong, X. Wang, Nanosized tin oxide as the novel material with simultaneous detection towards CO, H_2 and CH_4, Sens. Actuators, B 66 (2000) 225.

[18] G. Sberveglieri, Gas Sensors: Principles, Operation and Developments, 1992.

[19] I.T. Weber, A.P. Maciel, P.N. Lisboa-Filho, C.O. Paiva-Santos, W.H. Schreider, Y. Maniette, E.R. Leite, E. Longo, Effects of synthesis and processing on supersaturated rare earth-doped nanometric SnO_2 powders, Nano Lett. 2 (2002) 969.

[20] E.R. Leite, A.P. Maciel, I.T. Weber, P.N. Lisboa-Filho, E. Longo, C.O. Paiva-Santos, W.H. Schreider, Y. Maniette, C.A. Pascocimas, A.V.C. Andrade, Development of metal oxide nanoparticles with high stability against particle growth using a metastable solid solution, Adv. Mater. 14 (12) (2002) 905.

[21] S. Basu, P. Sujatha Devi, H. Maiti, Synthesis and properties of nanocrystalline ceria powders, J. Mater. Res. 19 (11) (2004) 3162.

[22] R. Tian, F. Zhao, F. Chen, C. Xia, Sintering of Samarium-doped ceria powders prepared by a glycine-nitrate process, Solid State Ionics 192 (2011) 580.

[23] C. Silveira, M.E. Lopes, M.R. Nunes, M.E. Melo Jorge, Synthesis and electrical properties of nanocrystalline $Ca_{1-x}Eu_xMnO_{3\pm\delta}(0.1 \leq x \leq 0.4)$ powders prepared at low temperature using citrate gel method, Solid State Ionics 180 (2010) 1702.

[24] J. Patil, D. Nadargi, J. Gurav, I. Mulla, S. Suryavanshi, Synthesis of glycine combusted $NiFe_2O_4$ spinel ferrite: a highly versatile gas sensor, Mater. Lett. 124 (2014) 144.

[25] J. Patil, D. Nadargi, I. Mulla, S. Suryavanshi, Spinel $MgFe_2O_4$ thick films: a colloidal approach for developing gas sensors, Mater. Lett. 213 (2018) 27.

[26] N. Rezlescu, C. Pasnicu, M.L. Craus, Effects of the rare-earth ions on some properties of a nickel-zinc ferrite, J. Phys. Condens. Matter 6 (1994) 5707.

[27] Z. Wang, L. Liu, Synthesis and ethanol sensing properties of Fe-doped SnO_2 nanofibers, Mater. Lett. 63 (2009) 917.